Cell Death and Differentiation (2012) 19, 1239–1252

www.nature.com/cdd

HDAC5 is required for maintenance of pericentric heterochromatin, and controls cell-cycle progression and survival of human cancer cells

P Peixoto[1,6], V Castronovo[1,6], N Matheus[1,6], C Polese[1,6], O Peulen[1,6], A Gonzalez[1,6], M Boxus[2], E Verdin[3], M Thiry[4,6], F Dequiedt[5,6] and D Mottet*[,1,6]

Histone deacetylases (HDACs) form a family of enzymes, which have fundamental roles in the epigenetic regulation of gene expression and contribute to the growth, differentiation, and apoptosis of cancer cells. In this study, we further investigated the biological function of HDAC5 in cancer cells. We found HDAC5 is associated with actively replicating pericentric heterochromatin during late S phase. We demonstrated that specific depletion of HDAC5 by RNA interference resulted in profound changes in the heterochromatin structure and slowed down ongoing replication forks. This defect in heterochromatin maintenance and assembly are sensed by DNA damage checkpoint pathways, which triggered cancer cells to autophagy and apoptosis, and arrested their growth both *in vitro* and *in vivo*. Finally, we also demonstrated that HDAC5 depletion led to enhanced sensitivity of DNA to DNA-damaging agents, suggesting that heterochromatin de-condensation induced by histone HDAC5 silencing may enhance the efficacy of cytotoxic agents that act by targeting DNA *in vitro*. Together, these results highlighted for the first time an unrecognized link between HDAC5 and the maintenance/assembly of heterochromatin structure, and demonstrated that its specific inhibition might contribute to increase the efficacy of DNA alteration-based cancer therapies in clinic.
Cell Death and Differentiation (2012) **19,** 1239–1252; doi:10.1038/cdd.2012.3; published online 3 February 2012

Histone deacetylases (HDACs) are enzymes that modulate the acetylation level of histones and non-histone proteins to regulate gene expression and chromatin structure. Eighteen human HDACs are divided into four classes: class I (HDAC1, 2, 3, 8); class II (HDAC4, 5, 6, 7, 9, 10), subdivided into class IIa (HDAC4, 5, 7) and class IIb (HDAC6 and 10); class III, also called sirtuin proteins (SIRT1–7); and class IV (HDAC11).[1] Several compounds were identified as broad-spectrum inhibitors of class-I and -II HDAC (HDACi).[2] These HDACis can cause cell-cycle arrest, activation of programmed cell death (apoptosis/autophagy), or inhibition of angiogenesis. Based on their potent anticancer effects *in vitro*, several HDACis are currently being investigated in clinical trials in cancer patients, both as single agents and in combination with other drugs. The FDA (Food and Drug Administration) approval of SAHA (suberoylanilide hydroxamic acid; Zolinza) for treatment of cutaneous T-cell lymphoma[3] validates the concept of HDAC inhibition to treat cancer.

Generally, HDACis are well tolerated when compared with most of the currently used antitumor treatments. However, some side effects have been reported. So, by targeting the most relevant HDAC members, it may be possible to improve efficacy by removing undesirable toxicities. Preclinical investigations by targeted knockdown of individual HDAC members demonstrated the roles of class IIa HDACs in tumorigenesis. Indeed, we and others have demonstrated that silencing of HDAC4 inhibited cancer cell proliferation *in vitro* and arrested tumor growth *in vivo* through epigenetic regulation of $p21^{WAF1/Cip1}$ gene expression.[4,5] Recently, Zhu *et al.*[6] also demonstrated HDAC7 is a crucial player in

[1]Metastasis Research Laboratory, University of Liège, Liège 4000, Belgium; [2]Cellular and Molecular Biology Unit, Gembloux Agro Bio-Tech (GxABT), Gembloux 5030, Belgium; [3]Gladstone Institute of Virology and Immunology, University of California San Francisco, San Francisco, CA 94158, USA; [4]Laboratory of Cell Biology, Department of Life Sciences, Faculty of Sciences, University of Liège, Liège 4000, Belgium; [5]Laboratoire de Signalisation et d'Interactions Protéiques (PSI), University of Liège, Liège 4000, Belgium and [6]Interdisciplinary Cluster for Applied Genoproteomics (GIGA), University of Liège, Liège 4000, Belgium
*Corresponding author: D Mottet, Metastasis Research Laboratory, GIGA-Cancer, University of Liège, Pathology Building, B23, + 4, Liège B-4000, Belgium.
Tel: + 32 4366 2488; Fax: + 32 4366 2975; E-mail: dmottet@ulg.ac.be
Keywords: histone deacetylases; cancer cells; siRNA; autophagy; cell proliferation; chemotherapy
Abbreviations: Akt, protein kinase B; Bax, Bcl-2-associated X; Bcl-2, B-cell lymphoma 2; BrdU, 5-bromo-2′-deoxyuridine; CAM, chorioallantoic membrane; CDK, cyclin-dependent kinase; CDKi, cyclin-dependent kinase inhibitor; Chk1, checkpoint kinase 1; Chk2, checkpoint kinase 2; Cip1, CDK-interacting protein 1; CldU, chlorodeoxyuridine; DMEM, Dulbecco's modified Eagle's medium; DNMT1, DNA methyltransferase 1; DSBs, double-strand breaks; DTT, dithiothreitol; E2F1, transcription factor E2F1; FACS, fluorescence-activated cell sorting; FBS, fetal bovine serum; FDA, Food and Drug Administration; FITC, fluorescein isothiocyanate; γ-H2AX, histone H2A.x phosphorylated on serine 139; HDAC, histone deacetylase; HDACi, histone deacetylase inhibitor; HP-1, heterochromatin protein 1; HRP, horseradish peroxidase; HSC70, heat-shock cognate 70-kDa protein; IdU, iododeoxyuridine; kip1, kinase-interacting protein 1; LC3, microtubule-associated protein 1A/1B-light chain 3; MCM, mini-chromosome maintenance protein; MEK2, MAPK/ERK kinase 2; MNaseI, micrococcal nuclease 1; Mus81, methyl methanesulfonate and ultraviolet-sensitive gene clone 81; NuRD, nucleosome-remodeling deacetylase complex; ORC, origin recognition complex; PBS, phosphate-buffered saline; PCNA, proliferating cell nuclear antigen; PI, propidium iodide; PI3K, phosphoinositide-3-kinase; pRb, retinoblastoma protein; RNAi, RNA interference; SA-β-gal, senescence-associated β-galactosidase; SAHA, suberoylanilide hydroxamic acid; SDS, sodium dodecyl sulfate; siRNA, small interfering RNA; SIRT, sirtuin; TSA, trichostatin A; WST-1, 2-(4-iodophenyl)-3-(4-nitrophenyl)-5-(2,4-disulfophenyl)-2H-tetrazolium, monosodium salt
Received 29.6.11; revised 28.11.11; accepted 04.1.12; Edited by H Ichijo; published online 03.2.12

cancer cell proliferation. Together, these findings would suggest that inhibition of class IIa HDACs might be a sufficient strategy to treat cancer. However, the contribution of HDAC5 to tumor progression is largely ignored and needs to be further characterized to determine whether class IIa HDAC members are the most relevant targets in cancer therapy.

The human HDAC5 gene is located on chromosome 17q21, a region which is characterized by losses of chromosomal material in different cancers.[7] Moreover, HDAC5 expression is frequently reduced in cancer such as colon cancer and acute myeloid leukemia,[8–10] and is associated with poor clinical outcome of lung cancer patients.[11] In contrary, an upregulation of HDAC5 has been observed in high-risk medulloblastoma and its expression is associated with poor survival.[12] Like for many HDACs, HDAC5 is then aberrantly expressed in tumors, suggesting that this HDAC may have a role in tumor progression.

Here, we investigated the function of HDAC5 in cancer cells. We found that its sub-nuclear localization changed during S phase progression, with HDAC5 colocalizing with actively replicating heterochromatic regions during late S phase. We demonstrated that its specific depletion by RNA interference (RNAi) induced a defect in pericentric heterochromatin assembly and slowed down an ongoing replication fork, which consequently induced DNA-damage checkpoint pathways, which leads to cell-cycle blocking, inhibition of cell proliferation, induction of apoptosis as well as autophagy, and, consequently, decreased tumor growth *in vivo*. Altogether, these findings implicate HDAC5 in the maintenance/assembly of pericentric heterochromatin structure and demonstrate that class IIa HDAC5 can represent a potential target for anticancer therapies.

Results

HDAC5 localizes to pericentromeric heterochromatin primarily during late S phase. To explore the function of HDAC5, we first examined its localization in HeLa cells. Confocal microscopy showed that approximately 85% of asynchronous cells showed a nuclear localization, with more intense foci around the nucleolus (Figure 1A). This localization was observed in different cell types, including MCF-7, MDA-MB-231, endothelial cells, and fibroblasts (data not shown). Transfection with two different efficient HDAC5 small interfering RNA (siRNA) correlated with loss of nuclear HDAC5 foci, excluding a non-specific staining (Supplementary Figures S1A, and S1B–S2). This localization was also confirmed with a second anti-HDAC5 antibody (Supplementary Figure S1C). To further characterize the intra-nuclear localization of HDAC5, we performed electron microscopy. Endogenous HDAC5 was detected as individual foci in the nucleus and the clusters showed a preferential colocalization of HDAC5 with pericentric (pericentromeric) heterochromatin (Figure 1B and Supplementary Figure S3). As fluorescence-activated cell sorting (FACS) analysis (see Figure 2a) revealed that an asynchronous population of HeLa cells is composed of 65–70% of cells in G_1, 20–25% of cells in S, and 5–10% of cells in G_2/M phase, we hypothesized that HDAC5 could target pericentric heterochromatin during different phases of the cell cycle. First, we monitored the localization and expression of HDAC5 during S phase. In early S phase, HDAC5 shows a diffuse nuclear staining, but in late S phase, the patterns were strikingly different, with HDAC5 now colocalizing with proliferating cell nuclear antigen (PCNA) to punctuate foci that are characteristic of late-replicating pericentric heterochromatin (Figure 1C). A colocalization between HDAC5 and heterochromatin protein 1 (HP-1), a heterochromatin marker, in late S phase confirmed that HDAC5 is localized to heterochromatic regions (Figure 1D). The re-entry into S phase was monitored by both FACS (see Figure 1C) and western blotting against cyclin E and phospho-histone H3 on Ser10, two markers of S phase progression,[13,14] a period during which the global level of HDAC5 did not change (Figure 1E). During mitosis, HDAC5 was not detectable with mitotic chromosome. However, we observed that HDAC5 also associated with heterochromatin in the G_1 phase (Supplementary Figure S4). Bearing in mind the importance of HDAC for chromatin condensation, we assessed the impact of HDAC5 depletion on the organization of pericentric heterochromatin by electron microscopy. Electron micrographs of GL3 siRNA/mock-transfected cells revealed dense nucleoli and a condensed pattern of heterochromatin. By contrast, HDAC5-depleted cells showed a reduced number of dense heterochromatin clusters at the periphery of the nucleolus, demonstrating failure of appropriate assembly/maintenance of chromatin structure at pericentric heterochromatin (Figure 1F). To determine whether HDAC5 depletion exerted a more global influence on chromatin organization, we performed a MNaseI (micrococcal nuclease 1) assay. No defects in wrapping of DNA by the histone octamer were observed in the absence of HDAC5 (Figure 1G), suggesting that HDAC5 did not have a role in the assembly/maintenance of nucleosome organization.

HDAC5 depletion affects DNA replication efficiency and cell-cycle progression. Because heterochromatin assembly and DNA replication are tightly coupled, we examined the consequences of HDAC5 depletion on DNA replication and S phase progression. To identify the effect of HDAC5 depletion on global S phase, asynchronous cells were transfected with an HDAC5 siRNA for 24, 48, and 72 h, and then pulsed with 5-bromo-2′-deoxyuridine (BrdU) before FACS analysis. After 24 h, the number of replicating cells in HDAC5-depleted cells was 28.8% lower compared with mock-transfected cells, and most of the cells were blocked in the G_1 phase (Figures 2a and b). Forty-eight hours after transfection, the percentage of replicating cells was significantly higher in HDAC5-depleted cells (28.23%) compared with control conditions (Figures 2c and d). After 72 h, no significant changes were observed (Figures 2e and f). These data show that HDAC5 siRNA-transfected cells are first blocked in G_1/S and then re-enter S phase later despite still efficient HDAC5 inhibition (Figure 2g). However, this reversible cell-cycle blocking was not observed in MCF-7 cells (data not shown).

To further investigate whether HDAC5 depletion altered cell-cycle progression, HDAC5-depleted cells were treated with the mitotic inhibitor nocodazole 24 h before harvesting

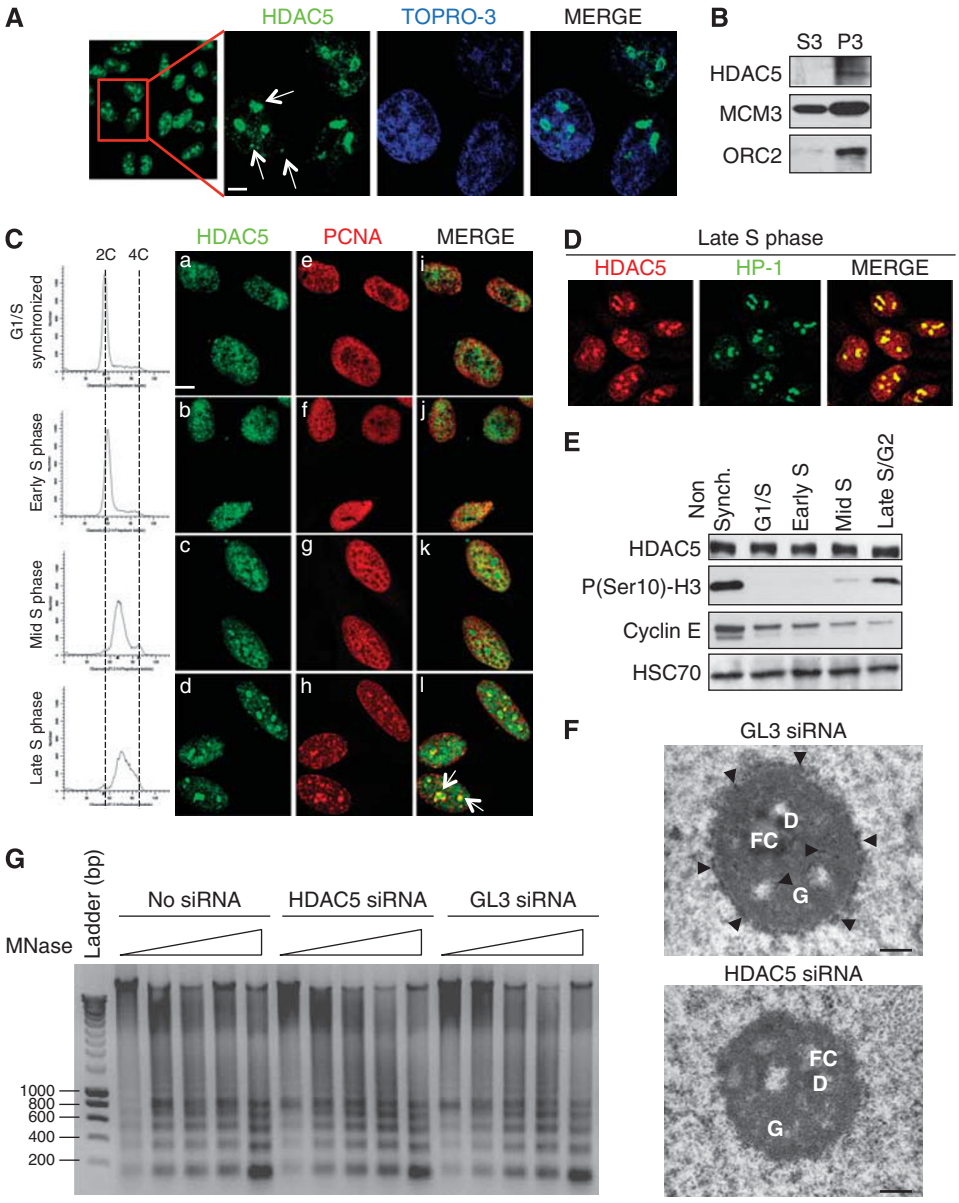

Figure 1 (**A**) Intracellular localization of endogenous HDAC5 protein in HeLa cells was addressed by indirect immunofluorescence and confocal microscopy using primary antibodies against HDAC5 recognized by secondary antibodies conjugated with Alexa 488 (green). DNA was counterstained with TOPRO-3 (blue) (original magnification: $\times$ 630; bar: 5 μm). The insets show individual cells from the field at a higher magnification. (**B**) HDAC5 is present in the fraction of chromatin-bound proteins. The fraction of chromatin-bound proteins was prepared as described under Materials and Methods, and the level of HDAC5 was assessed by western blotting. MCM3 and ORC2 proteins were used as fractionation control for the nuclear soluble proteins (S3) and the chromatin-enriched fraction (P3), respectively. (**C**) HDAC5 colocalized with heterochromatin in late S phase. Double immunostaining for HDAC5 (a–d) and PCNA (e–h), and merged images (i–l) in G_1/S (a, e and i) early S (b, f and j) mid-S (c, g and k), and late-S phase (d, h and l) (original magnification: $\times$ 630; bar: 5 μm). (**D**) HDAC5 colocalized with HP-1 in late S phase. Late-S phase cells were stained with an anti-HDAC5 antibody, followed by Alexa 546-conjugated secondary antibodies (red, top panel). The same cells were stained with an anti-HP-1 antibody, followed by an Alexa 488-conjugated secondary antibody (green, middle panel). The confocal merge image of HDAC5 and HP-1 staining shows colocalization (yellow, right panel) of HDAC5 and HP-1 in the nucleus (original magnification: $\times$ 630; bar: 15 μm). (**E**) Levels of HDAC5 protein during S phase progression. Whole-cell lysates were prepared from asynchronous, early S, mid-S, or late S phase, and the lysates were analyzed by western blotting using anti-HDAC5, anti-cyclin E, and anti-phosphoSer10 H3 antibodies. HSC70 was used as a loading control. (**F**) HDAC5 depletion alters chromatin structure. Electron microscopic analysis of MCF-7 cells transfected with either a GL3 siRNA or with an HDAC5 siRNA for 24 h. GL3 siRNA-transfected cells showed dense nucleoli and a condensed pattern of heterochromatin (black arrows). By contrast, HDAC5-depleted cells showed an even dispersion of the chromatin. FC, fibrillar center; D, dense fibrillar components; G, granular components (bar: 0.5 μm).(**G**) Nuclei extracted from MCF-7 cells transfected with No siRNA, GL3 siRNA, or with HDAC5 siRNA for 48 h were digested with increasing concentrations of MNase and analyzed by gel electrophoresis

(Figure 3a). Addition of nocodazole resulted in accumulation of cells in M phase in mock- or GL3 siRNA-transfected cells. By contrast, HDAC5 depletion led to a decreased number of cells in M phase after nocodazole treatment, in favor of an accumulation of cells in both G_1 and S phase. This demonstrated that HDAC5 depletion caused a defect in cell-cycle progression. However, after 48 or 72 h of transfection, HDAC5-depleted cells progressed through their cell cycle like

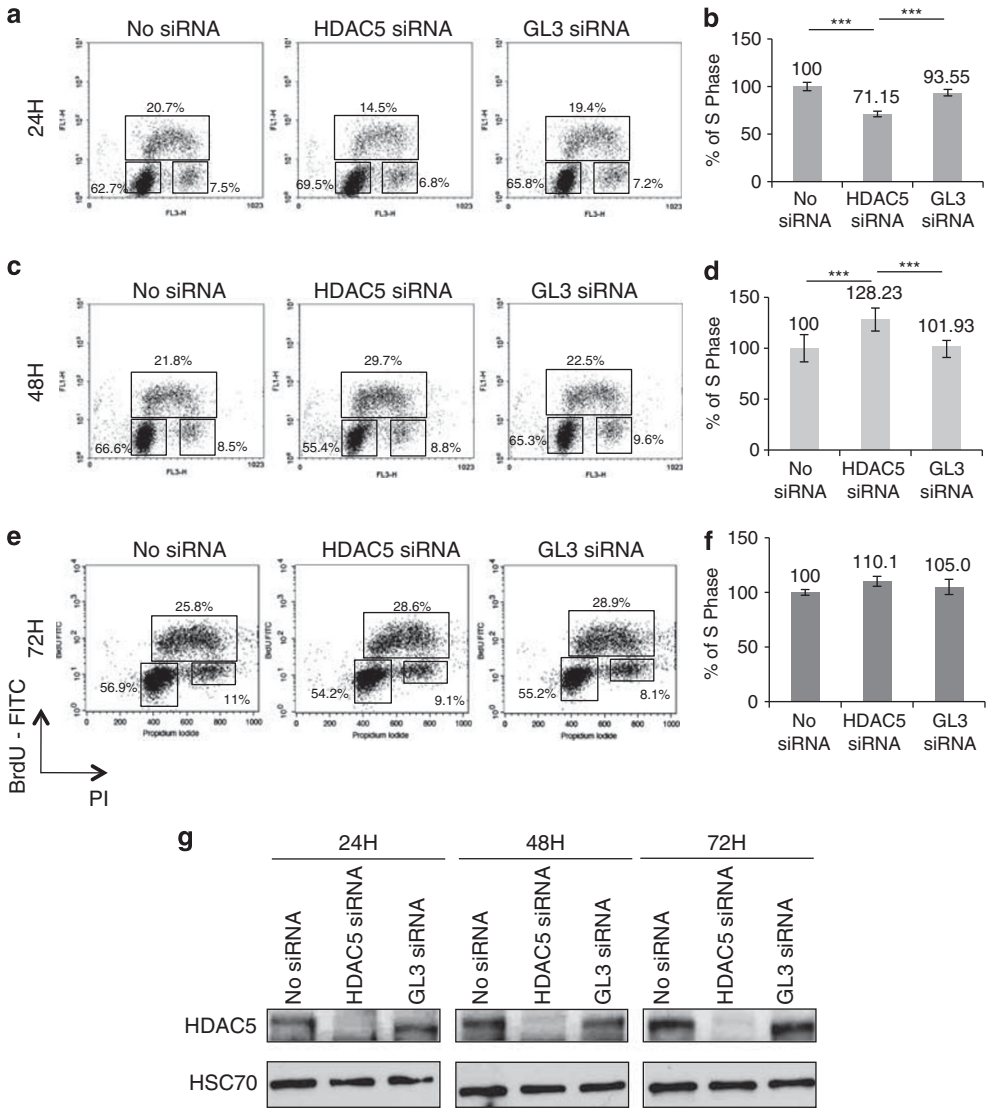

Figure 2 (**a–f**) HDAC5 depletion decreases DNA replication. HeLa cells were mock-transfected (No siRNA) or transfected with a siRNA directed against either HDAC5 or GL3 for 24 (**a**), 48 h (**c**), or 72 h (**e**); pulse-labeled for 30 min with the nucleotide analog BrdU; fixed; stained with an anti-BrdU antibody and PI; and analyzed by flow cytometry. The distributions of cell-cycle phases (G_1–S–G_2/M) are shown as percentage and are representative of three independent experiments. (**b**, **d** and **f**) In the bar graph, results are expressed as percentage of BrdU-positive cells arbitrarily fixed as 100% under the No siRNA condition. The values represent the mean ± S.D. of three independent experiments. Statistical analysis was performed by two-way ANOVA with a 95% interval of confidence followed by Bonferroni's post-test. ***$P<0.001$. (**g**) Western blot analysis of HDAC5 expression level in protein lysates from HeLa cells cultured in parallel

control cells, suggesting that cells seem to adapt or recover from HDAC5 loss, thus ensuring normal cell-cycle progression (Figure 3).

HDAC5 depletion inhibits replication fork progression. The inability to remove histones in front of the replication fork or to load nucleosomes behind the fork can impede replication progression. To test whether HDAC5 depletion affected replication fork progression, we performed DNA fiber assay (Figure 4a). A comparison of DNA fibers from control- and HDAC5 siRNA-transfected cells revealed a striking difference in the overall length of their replication tracks (Figure 4b) and stalled replication fork were commonly observed when HDAC5 is depleted (Supplementary Figure S5). When distribution of fibers length was quantified and plotted, the entire distribution of fiber length in HDAC5-depleted cells shifted leftward to shorter fibers (Figure 4c). Quantification of the doubly labeled fibers indicated that the average rate of fork progression in HDAC5-depleted cells was 1.26-fold slower than in control cells, suggesting that replication forks progressed at a slower rate in the absence of HDAC5 (Figure 4d).

DNA replication is a multi-step process, which first requires loading of DNA replication licensing factors. The chromatin association of ORC (origin recognition complex) and MCM (mini-chromosome maintenance protein) subunits, and PCNA, which are DNA replication licensing factors—was not altered in the absence of HDAC5 (Figure 4e), suggesting that replication factors were assembled normally and the replication defect occurred downstream from replication factor recruitment.

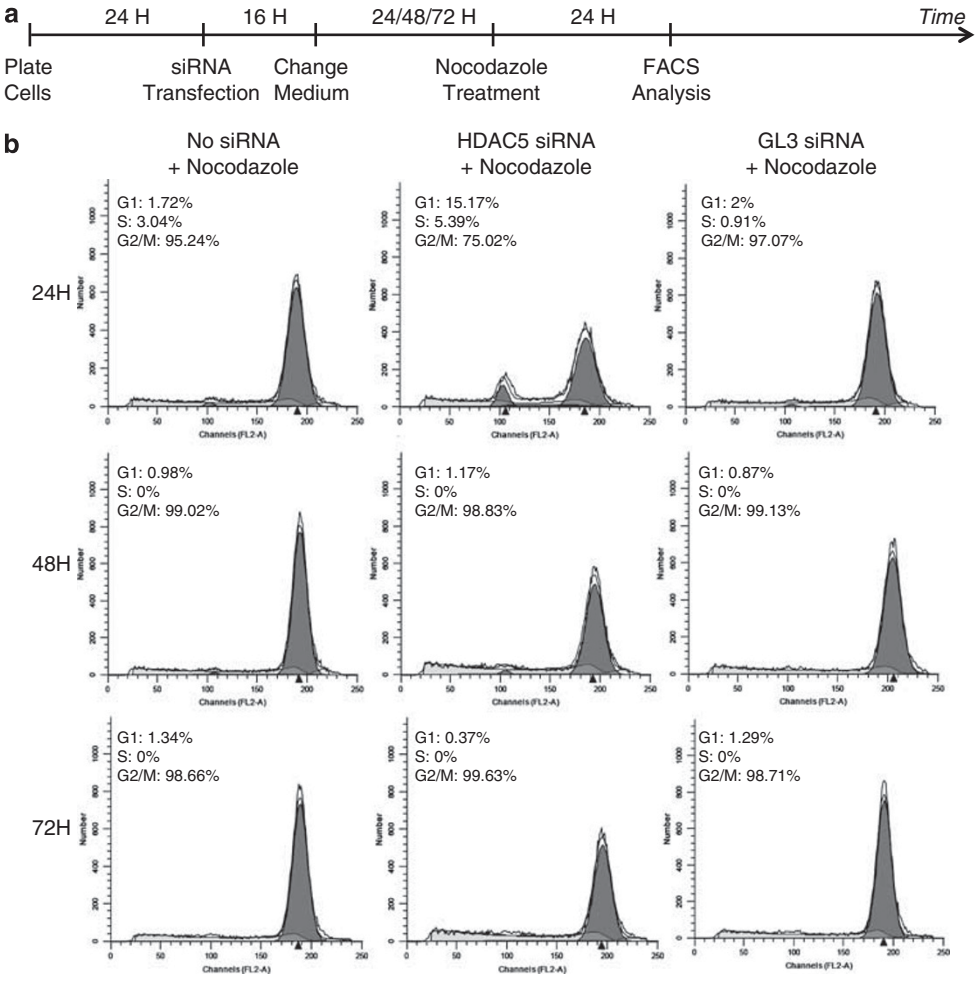

Figure 3 (**a** and **b**) HDAC5 depletion delays cell-cycle progression. HeLa cells were mock-transfected (No siRNA) or transfected with a siRNA directed against either HDAC5 or GL3 for 24, 48, or 72 h. Nocodazole, a mitotic inhibitor, was added 24 h before harvest. Samples were stained with PI and analyzed by flow cytometry. The distributions of cell-cycle phases (G_1–S.M) are shown as percentage and are representative of three independent experiments

Analysis of the activities of lamin B2, an early replication origin, and, Ors8, a late replication origin, demonstrated that HDAC5 depletion affected the firing of origins. Indeed, firing from both origins was reduced by approximately 40% at 24 h after transfection, whereas it was significantly increased after 48 h of transfection (Figures 4f and g).

HDAC5 depletion induces DNA damages and activates DNA-damage checkpoint pathways. Changes in heterochromatin structure alter fork progression. DNA double-strand breaks (DSBs) arise frequently as a consequence of replication fork stalling. One of the first molecules to appear following DSB formation is the phosphorylated form of H2AX histone variant on Serine^{139} (γ-H2AX). Inhibition of HDAC5 expression led to a significant increase in γ-H2AX as early as 24 h after transfection as shown by western blotting and single-cell electrophoresis assay (Figures 5a and b), suggesting that HDAC5 depletion leads to DNA damages. A co-staining between γ-H2AX and BrdU revealed that these DNA damages occur at replication sites mainly in mid- to late S phase (Figure 5c and Supplementary Figure S6).

DNA damages during S phase activate the intra-S phase checkpoint and involve transducer kinases such as checkpoint kinase 1 (Chk1) and/or Chk2.[15,16] The active form of Chk1 but not Chk2 was detected in HDAC5-depleted cells. The level of p53, a downstream target of Chk1, is slightly increased 24 h after HDAC5 depletion, but it declined thereafter, and reached the basal level after 32 h. In HDAC5-depleted cells, the p53 target gene p21$^{WAF1/Cip1}$ also showed a similar rise and fall, although it faded off more slowly. Similarly, upregulation of p27^{kip1} and p16INK4A, two other cyclin-dependent kinase (CDK) inhibitors (CDKi), was transient and not sustained over time. As attempted, these CDKis inhibit the phosphorylation of retinoblastoma protein (pRb), thereby preventing E2F1 from transcribing genes that are required for cell-cycle progression such as cyclin A or E2F1 itself (Figure 5d). However, induction of these CDKis and accumulation of hypo-phosphorylated pRB were not maintained after 72 or 96 h (Figure 5e), showing that HDAC5 depletion caused a transient induction of CDKis that decline slightly at basal level later.

To see whether induction of both p53 and p21$^{WAF1/Cip1}$ was similar in other cell types, we explored the consequences of

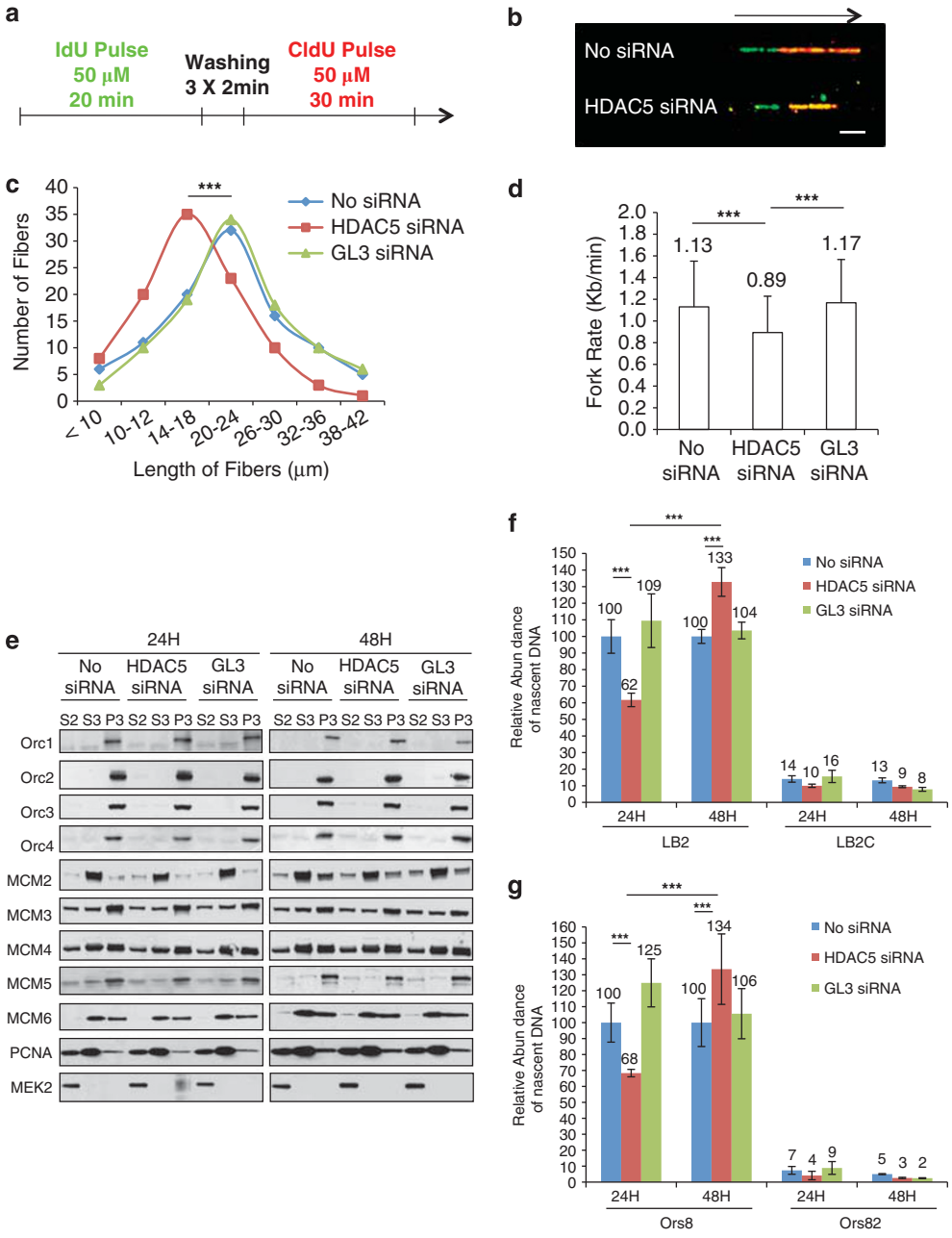

Figure 4 (**a–d**) HDAC5 depletion inhibits replication forks. (**a**) A schematic representation showing the principle of the DNA fiber assay. (**b**) Representative images of replication tracks in mock (No siRNA)- and HDAC5 siRNA-transfected cells pulse-labeled with 50 μM IdU for 20 min (green track) followed by 50 μM CldU for 30 min (red track), and then processed for DNA fiber spreads as described under Materials and Methods. Fork direction is indicated by a black arrow. All track photos are shown at identical magnifications (original magnification: $\times$ 630; bar: 5 μm). (**c**) The numbers of fibers for each specified length in mock (No siRNA)-, HDAC5 siRNA-, and GL3 siRNA-transfected cells were compared. The data were derived from one of two independent experiments in which at least 100 fibers were analyzed per experiment. Results are expressed as a frequency distribution of fiber length. Fiber length means were compared by one-way ANOVA with a 95% interval of confidence followed by Bonferroni's post-test. (**d**) Mean fork rates (kb/min) $\pm$ S.D. in each condition were calculated from the data shown in panel **c**, and compared by one-way ANOVA with a 95% interval of confidence. (**e**) HDAC5 depletion does not alter the chromatin loading of DNA replication licensing factors. HeLa cells were mock-transfected (No siRNA) or transfected with a siRNA directed against either HDAC5 or GL3 for 24 or 48 h. Fractions of chromatin-bound proteins were prepared as described under Materials and Methods, and the level of different DNA replication licensing factors was assessed by western blotting. The MEK2 protein was used as a fractionation control. S2, cytoplasmic fraction; S3, nuclear soluble proteins; P3, chromatin-enriched fraction. (**f** and **g**) HDAC5 depletion inhibits the firing of origins. Histogram plots of the lamin B2 (**f**) and Ors8 (**g**) origin activities in mock-transfected cells or cells transfected with a siRNA directed against either HDAC5 or GL3 for 24 or 48 h as measured by nascent-strand DNA abundance. Results are expressed as a percentage of the nascent-DNA strand abundance mean under the No siRNA condition. The values represent the mean $\pm$ S.D. of two independent experiments, each with three technical replicates. Statistical analysis was performed by two-way ANOVA with a 95% interval of confidence followed by Bonferroni's post-test. ***$P<0.001$

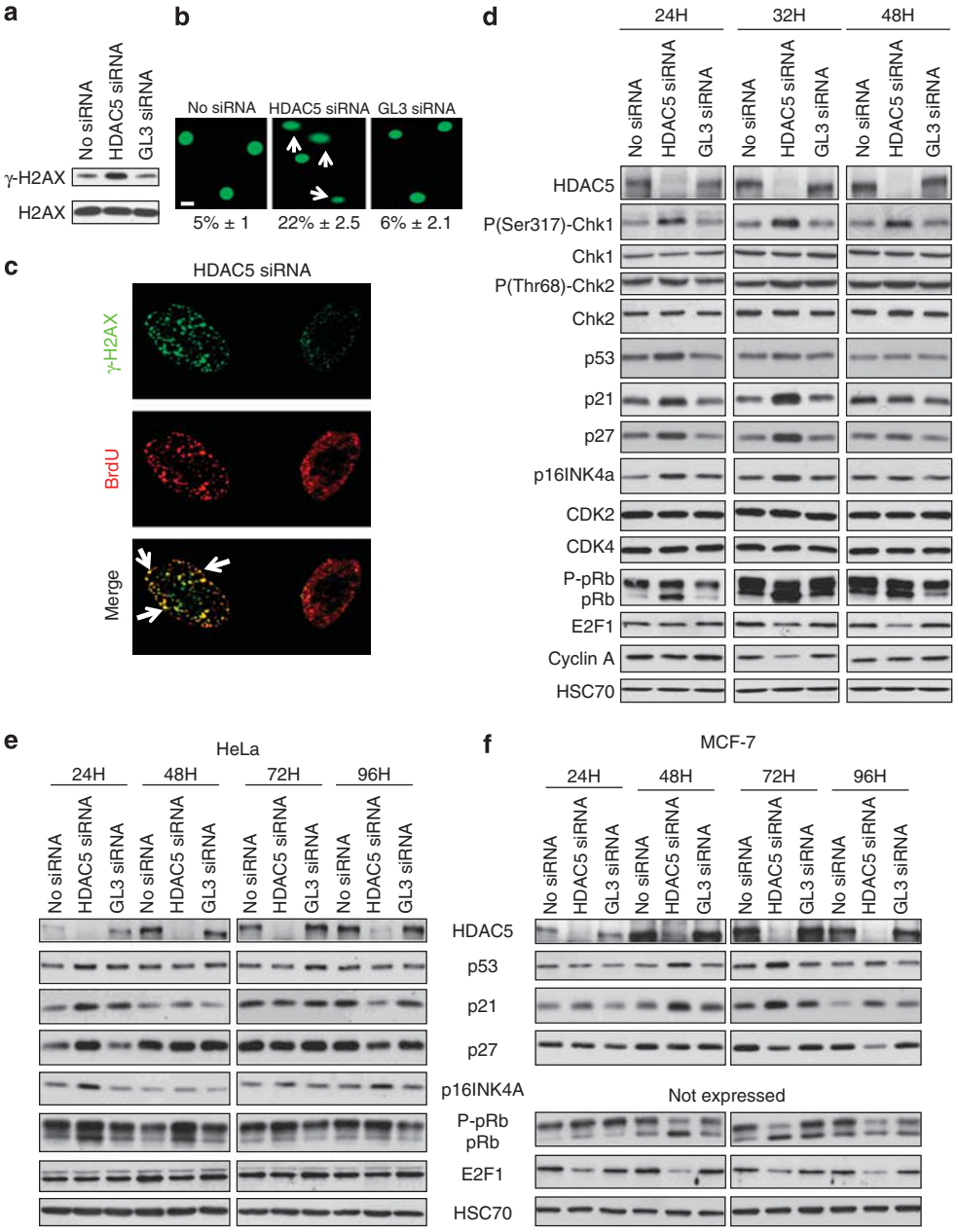

Figure 5 HDAC5 depletion leads to DNA damages and activates the DNA-damage checkpoint pathway. (**a**) HeLa cells were mock-transfected (No siRNA) or transfected with a siRNA directed against either HDAC5 or GL3 for 24 h, and western blotting was performed using anti-γ-H2AX antibodies. (**b**) HeLa cells were mock-transfected (No siRNA) or transfected with a siRNA directed against either HDAC5 or GL3 for 24 h, and the presence of DNA damages was assayed by the Oxiselect Comet Assay Kit according to the manufacturer's instructions (Cellbiolabs, San Diego, CA, USA). Representative cells are shown for each condition. A higher number of nuclei in HDAC5-depleted cells showed the presence of the characteristic comet tail, indicating the presence of DNA damages. The arrows indicate cell nuclei with tail (original magnification: × 630; bar: 10 μm). The average comet tail moment length was scored for at least 100 nuclei per slide by using the CASP software, version 1.2.2 (www.casp.of.pl). Results are expressed as mean ± S.D. and are indicated under the pictures. (**c**) HeLa cells were transfected as in panel **a**, pulse-labeled for 30 min with the nucleotide analog BrdU, fixed, and double immunostained for γ-H2AX (green) and BrdU (red). Representative pictures of HDAC5-depleted cells from two independent experiments are shown. The white arrows indicate colocalization foci into the nucleus. (**d**) HeLa cells were mock-transfected (No siRNA) or transfected with a siRNA directed against either HDAC5 or GL3 for 24, 32 or 48 h. Total protein extracts were prepared and processed for western blotting using the indicated antibodies. HSC70 was used as a loading control. HeLa cells (**e**) or MCF-7 cells (**f**) were mock-transfected (No siRNA) or transfected with a siRNA directed against either HDAC5 or GL3 for 24, 48, 72, or 96 h. Total protein extracts were prepared and processed for western blotting using the indicated antibodies. HSC70 was used as a loading control

HDAC5 depletion in MCF-7 cells, which also harbors wild-type p53 and pRb genes. In those cells, HDAC5 depletion also induced activation of the p53–p21$^{WAF1/Cip1}$ and pRb pathways, but the induction was more persistent compared with HeLa cells (Figure 5f).

HDAC5 depletion induced both apoptosis and autophagy. HDAC5 depletion induced a DNA-damage response, which engages both the p53–p21$^{WAF1/Cip1}$ and the p16INK4A–pRb pathways. These pathways can establish and maintain the growth arrest that is typical

of senescence and/or induce apoptosis. Any blue staining indicative of SA-β-gal (senescence-associated β-galactosidase) activity, a typical marker of senescence, was observed in both HeLa and MCF-7 cells in the absence of HDAC5 (data not shown). However, HDAC5 depletion drives cells into apoptosis. By 48 h after transfection, there was a nearly two-fold increase of cells undergoing apoptosis (Figures 6a and b). Apoptosis in both cell types was confirmed by caspase-7 activation (Figures 6c and d, and Supplementary Figures S7A and S7B) as well as microscopic analysis showing typical apoptotic morphology (Supplementary Figure S8).

As autophagy and apoptosis can share common components and inhibitory/activating signaling pathways, we next determined whether HDAC5 depletion could also induce autophagy by analyzing the level of LC3, an autophagosomal marker. LC3-II levels (compared with β-actin loading controls) increased in both HeLa and MCF-7 cells depleted for HDAC5 (Figures 6c and d, bottom panels), suggesting concomitant induction of apoptosis and autophagy. This amount of LC3-II further accumulates in the presence of a lysosomal inhibitor, indicating enhancement of the autophagic flux (Supplementary Figure S9A). To further confirm activation of autophagy, both HeLa and MCF-7 cells were stained with an LC3 antibody

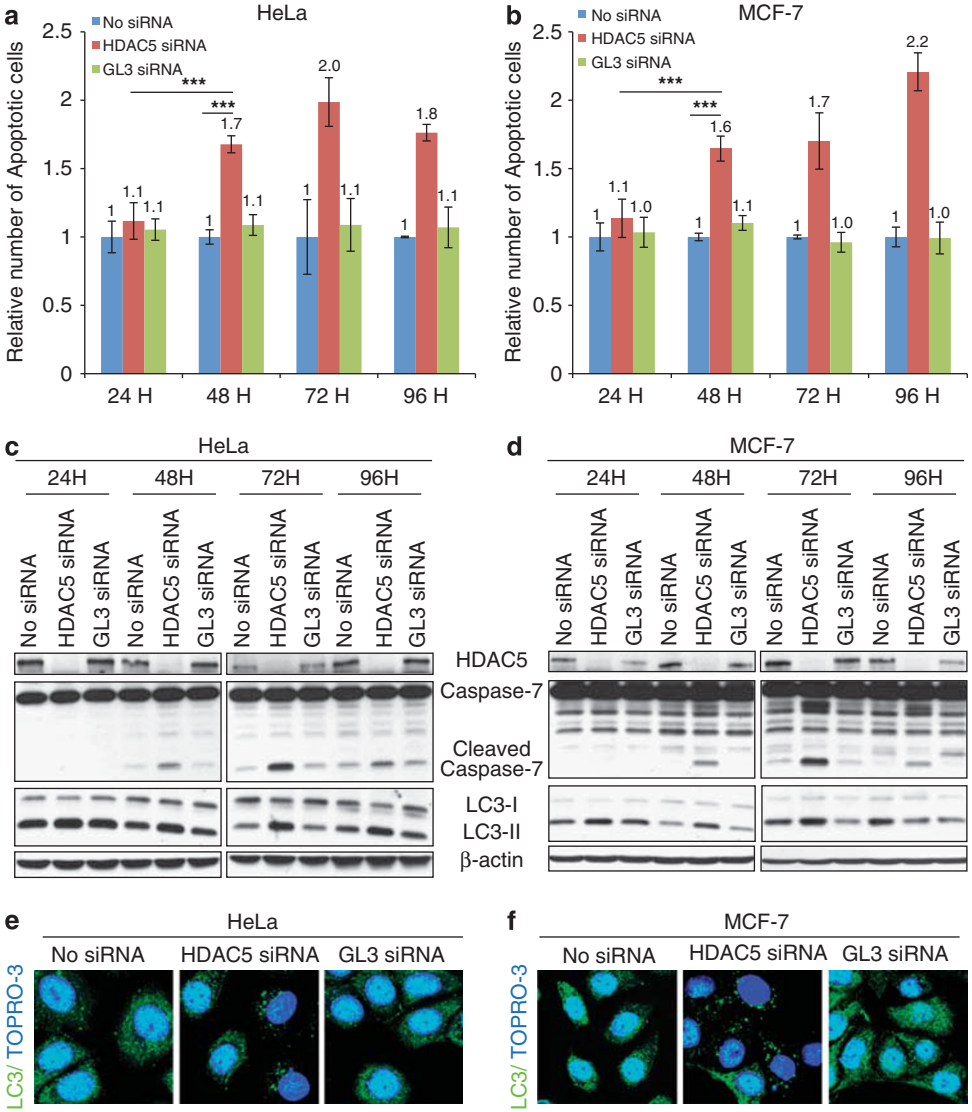

Figure 6 HDAC5 depletion induces both apoptosis and autophagy. HeLa (**a**) or MCF-7 cells (**b**) were mock-transfected (No siRNA) or transfected with a siRNA directed against either HDAC5 or GL3 for 24, 48, 72, and 96 h. Apoptotic cells were quantified by Annexin V staining as described under Materials and Methods. Results are presented as a relative number of apoptotic cells arbitrarily fixed as1 under the No siRNA condition. The values represent the mean ± S.D. of three independent experiments. Statistical analysis was performed by two-way ANOVA with a 95% interval of confidence followed by Bonferroni's post-test. ***$P<0.001$. HeLa (**c**) or MCF-7 cells (**d**) were mock-transfected (No siRNA) or transfected with a siRNA directed against either HDAC5 or GL3 for 24–48–72 or 96 h. Both floating and adherent cells were collected and lysed. Western blotting was performed using anti-HDAC5, anti-caspase-7, and anti-LC3 antibodies. β-Actin was used as a loading control. (**e** and **f**) Both HeLa and MCF-7 cells were mock-transfected (No siRNA) or transfected with a siRNA directed against either HDAC5 or GL3 for 48 h. Autophagic vacuoles (white arrows) were detected by confocal microscopy after LC3 staining. Representative cells are shown for each condition (original magnification: × 630; bar: 5 μm)

and presence of autophagic vacuoles was analyzed by confocal microscopy. Figures 6e and f showed the presence of autophagic vacuoles in both HeLa and MCF-7 depleted for HDAC5. This formation/accumulation of autophagic vacuoles was confirmed by electron microscopy (Supplementary Figure S9B).

HDAC5 depletion globally reduces cancer cell proliferation, survival, and inhibits tumor growth *in vivo*. Because HDAC5 depletion affects cell-cycle progression, and induces both apoptosis and autophagy, we assessed the effect of HDAC5 depletion on the global cancer cell proliferation, survival, and tumor growth. *In vitro*, HDAC5 depletion significantly decreased proliferation (Figures 7a and b) as well as survival (Figures 7c and d) of both HeLa and MCF-7 cells. To examine the effect of HDAC5 depletion on tumor cell growth, we used an *in vivo* model in which cancer cells are engrafted onto embryonated chick chorioallantoic membrane (CAM). Tumors formed from HDAC5-depleted MCF-7 cells (Figures 7e–g) were smaller than control tumors, demonstrating the relevance of inhibiting HDAC5 in cancer cells *in vivo*.

HDAC5 depletion increases the efficacy of chemotherapeutic drugs *in vitro*. It has become increasingly clear that the chromatin compaction present in heterochromatin helps to protect DNA from damaging drugs.[17] As such, knockdown of heterochromatic proteins or induced de-condensation of chromatin sensitizes cells to DNA damages.[18] According to our data, HDAC5 depletion could expose heterochromatic regions to DNA-damaging drugs. Therefore, we examined whether HDAC5 depletion could sensitize cancer cells to chemotherapeutic drugs. MCF-7 or HeLa cells were transfected with a siRNA against HDAC5 for 24 h, and then incubated either with doxorubicin or cisplatin for an additional 24 h. Loss of HDAC5 caused 5–6 times more apoptosis compared with cisplatin or doxorubicin alone in HeLa cells (Figures 8a–c). Interestingly, the combination of HDAC5 siRNA/doxorubicin or cisplatin produces more cell death than chemotherapeutic drugs associated with trichostatin A (TSA), a broad-spectrum HDACi (Supplementary Figures S10A and S10B), demonstrating that only inhibition of HDAC5 produces better cytotoxicity than HDACi to potentiate chemotherapeutic drugs.

Using the same schedule, HDAC5 depletion in MCF-7 cells did not potentiate the activity of chemotherapeutic drugs. To test whether this schedule alters the effectiveness of combination treatment, HDAC5-depleted MCF-7 cells were exposed to DNA-damaging drugs 48 h after siRNA transfection for an additional 24 h. A better cytotoxic/apoptotic effect was observed (Figures 8d and e, and Supplementary Figure S10C) suggesting that appropriate sequencing and scheduling of the combination of HDAC5 silencing with DNA-damaging drugs is required for each cancer cell type.

Discussion

The inheritance and faithful maintenance of chromatin organization is crucial for eukaryotic cells. To orchestrate DNA replication in the context of chromatin, cells have evolved efficient nucleosome dynamics involving assembly pathways and chromatin maturation mechanisms. During replication, modified parental histones are displaced ahead of the replication fork and are randomly distributed between the two daughter strands. Concomitantly, deposition of *de novo*-synthesized histones H3 and H4 provides the full complement of histones that are needed to ensure proper assembly of the duplicated material. During its initial synthesis, histone H4 is acetylated at lysine residues 5 and 12. These residues must be deacetylated to form heterochromatin in late S phase, thus ensuring secure maintenance of the under-acetylated state of heterochromatin. This latter step is promoted through the action of HDAC-containing complexes such as Mi-2/NuRD (nucleosome-remodeling deacetylase complex) and/or the Sin3/HDAC chromatin-modifying complex,[19] which have been shown to contain both HDAC1 and HDAC2, and associate with pericentric heterochromatin during S phase.[20,21] Whereas some reports pointed to the role of HDAC2 in the rearrangement of the nucleosomes during the formation of heterochromatin in late S phase,[22] as well as the implication for HDAC3 in replication fork progression,[23,24] we demonstrated that HDAC5 is recruited to heterochromatin regions, probably with members of NuRD/Sin3 chromatin remodeling complexes as well as with other epigenetic regulators such as DNA methyltransferase 1 (DNMT1) or HP-1,[22,25–28] to participate in the establishment of the pericentric heterochromatin structure in late S phase. However, the mechanisms of action of HDAC5 in the assembly/maturation of pericentric heterochromatin remain to be identified.

The chromatin structural defect caused by HDAC5 depletion results in a slow-growth phenotype, with delayed cell-cycle progression and activation of multiple checkpoints pathways. We indeed observed: (i) activation of the Chk1-dependent intra-S phase checkpoint, which could survey alterations in chromatin structure, and serves as an efficient mechanism to slow down fork progression in the absence of appropriate chromatin assembly and block initiation of new replication forks in a global manner, consistent with reports showing that origin firing is inhibited during S phase when DNA damage or replication fork stalling activates the intra-S-phase checkpoint kinases;[29–31] and (ii) activation of a G_1/S checkpoint pathway, which prevents late-G_1 cells from entering the S period by directly or indirectly inhibiting initiation at the earliest-firing origins, with the consequence that the entire S period is delayed along the cell-cycle axis.[29,30]

In addition to cell-cycle blocking, we also observed activation of autophagy in HDAC5-depleted cells. Numerous studies suggest that autophagy may function in the regulation of cell survival and have a major role in the maintenance of genomic integrity.[32] The precise role of autophagy in response to HDAC5 depletion is not fully understood yet but is thought to be a temporary survival mechanism, which delays apoptosis as inhibition of HDAC5 silencing-induced autophagy unmasks and accelerates apoptosis (data not shown).

Activation of checkpoint pathways and consequently cell-cycle blocking in HDAC5-depleted cells should allow time for the chromatin defects to be resolved. Once repair is accomplished, these checkpoint/repair pathways are usually

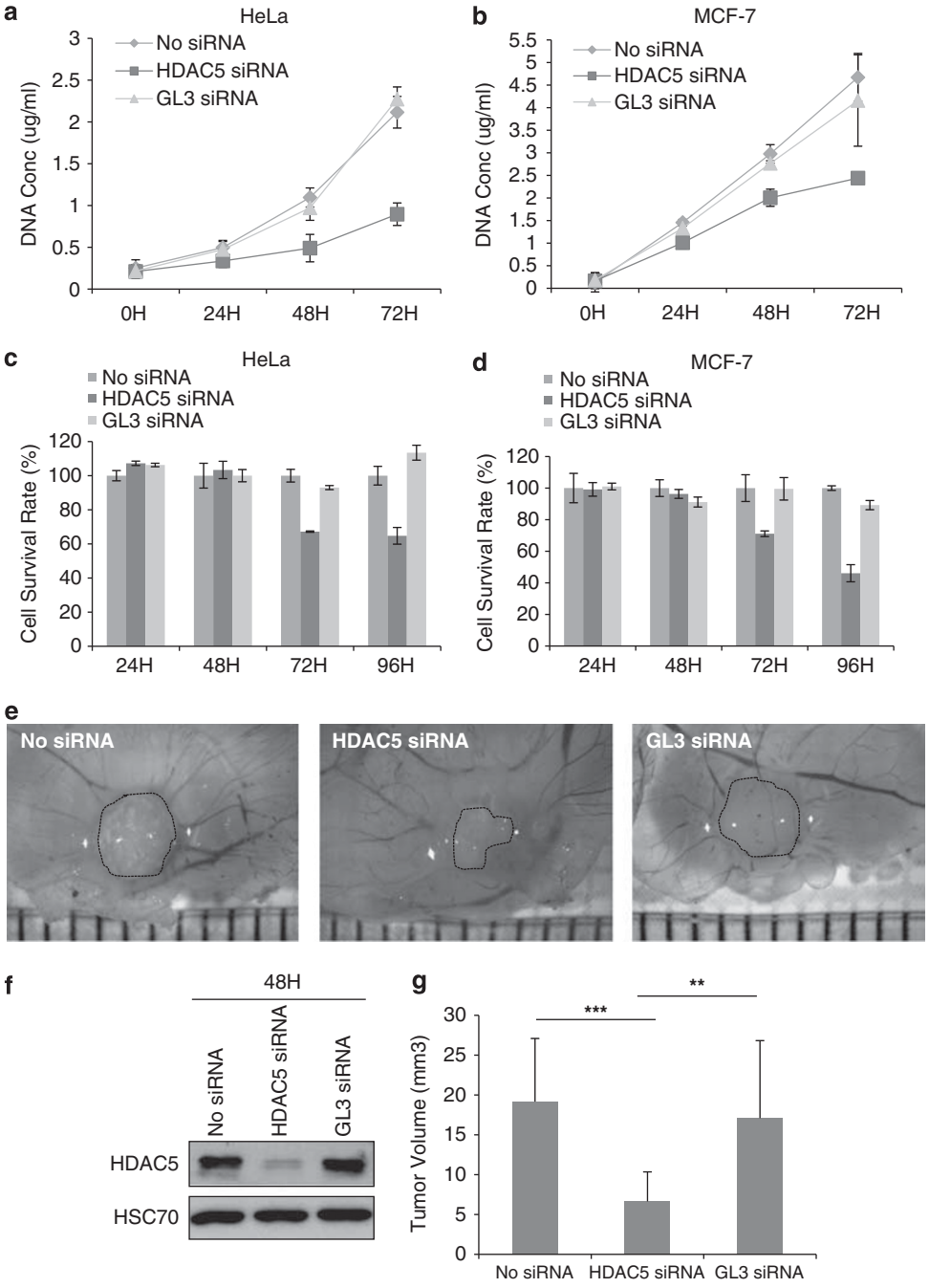

Figure 7 HDAC5 depletion blocks cancer cell proliferation, decreases cell survival, and inhibits tumor growth *in vivo*. HeLa (**a**) or MCF-7 cells (**b**) were mock-transfected (No siRNA) or transfected with a siRNA directed against either HDAC5 or GL3 for 24–48 and 72 h. Time-course analysis of DNA content was performed by fluorimetric DNA titration. The values are the mean ± S.D. of three replicates and are representative of three separate experiments. Both HeLa (**c**) and MCF-7 (**d**) cells were mock-transfected (No siRNA) or transfected with a siRNA directed against either HDAC5 or GL3 for 24–48–72 and 96 h. WST-1 cell survival assay was performed as described under Materials and Methods. The values are the mean ± S.D. of three replicates and are representative of three separate experiments. (**e**) MCF-7 cells were mock-transfected (No siRNA) or transfected with an HDAC5 or a GL3 siRNA, implanted on CAM 16 h later, and inoculated 7 days. A representative photograph of a 'No siRNA' tumor, an 'HDAC5 siRNA' tumor, and a 'siRNA GL3' tumor. The dotted lines indicate tumor boundaries at the end of the experiment. (**f**) In parallel, a fraction of transfected MCF-7 cells was plated and maintained in culture during the 48 h period. Total protein extracts were prepared from those cells and processed for western blotting using anti-HDAC5 antibodies. HSC70 was used as a loading control. (**g**) Volume of tumors resected 7 days after inoculation was calculated. The values are the mean ± S.D. of at least six tumors in each group and are representative of two separate experiments. Statistical analysis was performed by one-way ANOVA with a 95% interval of confidence followed by Bonferroni's post-test. $^{**}P<0.01$, $^{***}P<0.001$

silenced so that cell-cycle progression is allowed to resume. In HDAC5-depleted HeLa cells, we noticed resumption of normal cell-cycle progression after transient cell-cycle blocking as demonstrated by biphasic modulation of cell-cycle inhibitors such as $p21^{WAF1/Cip1}$, $p27^{kip1}$, or P-pRb, which occurs in conjunction with release from cell-cycle blocking.

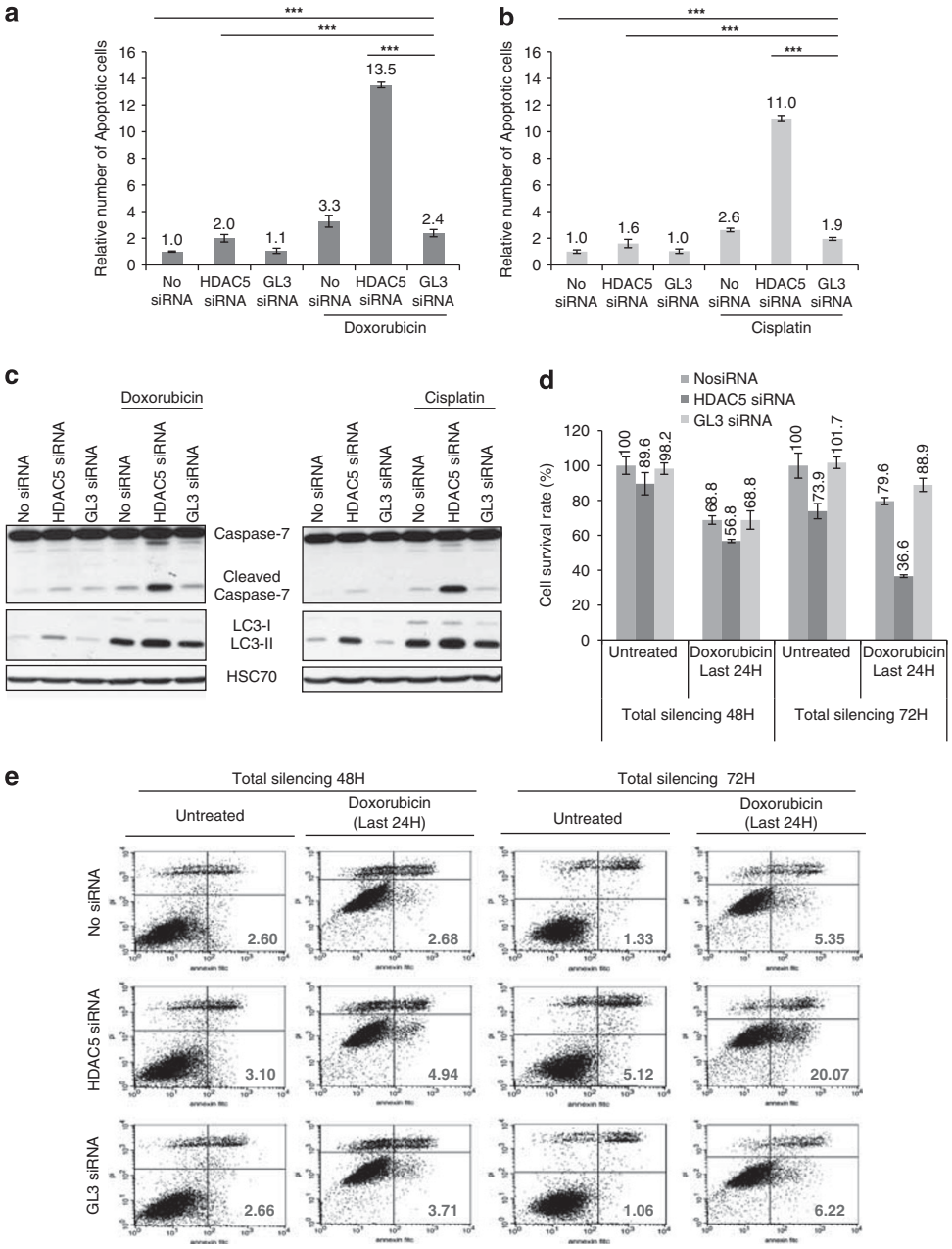

Figure 8 HDAC5 depletion sensitizes both HeLa and MCF-7 cells to chemotherapeutic agents. (**a** and **b**) HeLa cells were mock-transfected (No siRNA) or transfected with a siRNA directed against either HDAC5 or GL3 for 24 h and then treated either with doxorubicin (2 μM) (**a**) or cisplatin (7 μM) (**b**) for an additional 24 h. Apoptotic cells were quantified by Annexin V staining as described under Materials and Methods. ***$P<0.001$. (**c**) HeLa cells were transfected as in panels **a** and **b**. Both floating and adherent cells were collected and lysed. Western blotting was performed using anti-caspase-7 and anti-LC-3 antibodies. HSC70 was used as a loading control. (**d**) MCF-7 cells were mock-transfected (No siRNA) or transfected with a siRNA directed against either HDAC5 or GL3 for 24 or 48 h, and then treated with doxorubicin (2 μM) for an additional 24 h. WST-1 cell survival assay was performed as described under Materials and Methods. (**e**) MCF-7 cells were transfected as in panel **d**. Apoptotic cells were quantified by Annexin V staining. For each condition, representative FACS dot plots are presented with number of cells in Annexin V^+/PI^- quadrant

This transient cell-cycle arrest suggests that either checkpoint recovery (fulfillment of the requirement) or checkpoint adaptation occurs in HDAC5-depleted HeLa cells. In the light of an yeast two-hybrid screen showing interaction between HDAC5 and Mus81 (methyl methanesulfonate and ultraviolet-sensitive gene clone 81), we are actually investigating the role of this endonuclease Mus81 on cell-cycle resumption. Preliminary experiments demonstrated the possible implication of Mus81 in the checkpoint recovery/adaptation of cells from HDAC5 depletion stress, allowing them to survive and proliferate with apparently intact chromosomes or at the cost of tolerating mutation. As defective DNA-damage repairs with Mus81 mutations are often observed in breast cancer patients,[33] we hypothesized that MCF-7 cells harbor mutations in gene encoding Mus81 and/or other DNA repair/checkpoint proteins that impair checkpoint recovery/adaptation,

leading to excessive unrepaired chromatin defects and consequently apoptosis.

After an initial attempt to recover or adapt, prolonged HDAC5 inhibition in HeLa cells overwhelms the cells and results in apoptosis, suggesting that either chromatin defects are too severe or recovery/adaptation mechanisms are followed by excessive genome instability, leading to cell death in subsequent cell cycles for a subpopulation of cells. In addition to activation of the apoptotic program, we noted that autophagy is still induced at late time point in the time course of HDAC5 depletion. Despite its initial role as a survival pathway, progressive autophagy can result in cell death if allowed to proceed to completion under persistent stress and therefore, both processes would cooperate to lead to cell death.

The role of HDAC5 in heterochromatin assembly and maturation also has an impact in DNA alteration-based cancer strategies. Consistent with others studies,[34,35] we reported here that HDAC5 depletion potentiates the effect of chemotherapeutic agents that target DNA by inducing heterochromatin de-condensation, thereby facilitating access of drugs to DNA. Despite a more accessible chromatin in both cell types, we found that a different sequencing and scheduling of the combination of HDAC5 silencing with DNA-damaging drugs is required for each cancer cell types. Why did HDAC5-depleted MCF-7 cells show a delayed death response to DNA-damaging drugs compared with HeLa cells? In MCF-7 cells, several factors such as caspase-3 deficiency, levels and activity of the Bax (Bcl-2-associated X)/Bcl-2 (B-cell lymphoma 2) proteins, or activation of phosphoinositide-3-kinase (PI3K)/Akt (protein kinase B) kinases can contribute to refractory to apoptosis induced by DNA-damaging drugs. Autophagy also represents a mechanism of resistance to modalities, which affect DNA. Because induction of autophagy delays apoptosis in the absence of HDAC5 only, we are currently focusing our research to further understand the impact of autophagy in the death response of HDAC5-depleted cells treated with chemotherapeutic agents.

Altogether, our findings revealed that HDAC5 is a regulator of pericentric heterochromatin assembly, and demonstrated that its inhibition alone or in combination with chemotherapeutic agents might represent a promising strategy in cancer therapy.

Materials and Methods

Cell culture, synchronization, and treatment. HeLa cells were maintained in Dulbecco's modified Eagle's medium (DMEM) with 10% heat-inactivated fetal bovine serum (FBS). MCF-7 cells were maintained in α-Modified Eagle's Medium (αMEM) supplemented with 10% heat-inactivated FBS. Synchronization was achieved by treating cells with 2 mM hydroxyurea (Sigma) and 200 μg/ml nocodazole (Sigma, St. Louis, MO, USA). TSA, cisplatin and doxorubicin were purchased from Sigma.

Antibodies. Anti-FLAG and anti-BrdU (clone BU-33) antibodies were purchased from Sigma. Anti-BrdU (clone BU1/75), anti-ORC1, anti-ORC3, and anti-ORC4 antibodies were from AbDSerotec (Kidlington, UK). Anti-HDAC5, anti-p16INK4A, anti-MCM2, anti-MEK2 (MAPK/ERK kinase 2), anti-ORC2, anti-Chk1, anti-phosphoSer317 Chk1, anti-Chk2, anti-phosphoThr68 Chk2, and anti-caspase-3/7 antibodies were purchased from Cell Signaling (Carlsbad, CA, USA). Anti-HDAC5, anti-histone H2AX, anti-phosphoSer139 histone H2AX and anti-phosphoSer10 histone H3 antibodies were from Millipore (Bedford, MA, USA). Anti-BrdU (clone B44), anti-MCM4, anti-MCM5, anti-MCM6, anti-p27, anti-pRb, anti-cyclin E, and anti-cyclin A antibodies were purchased from BD Biosciences (Erembodegem, Belgium). Anti-p53 antibodies were from Upstate Biotechnology (Lake Placid, NY, USA). Anti-p21$^{WAF1/Cip1}$, anti-E2F1, anti-MCM3, anti-Cdc6, anti-PCNA (clone PC10), anti-HP-1, anti-HDAC5, and anti-HSC70 (heat-shock cognate 70-kDa protein) were purchased from Santa Cruz Biotechnology (Santa Cruz, CA, USA). Anti-LC3 antibodies were purchased from Abgent (San Diego, CA, USA).

siRNA transfection. siRNAs were synthesized either by Eurogentec (Liège, Belgium) or Dharmacon (Lafayette, CO, USA). Calcium phosphate-mediated transfections were performed as described previously.[36]

Immunocytochemistry. After fixation and permeabilization, cells were incubated with primary antibodies and with corresponding Alexa dye-conjugated secondary antibodies (Molecular Probes, Eugene, OR, USA) and mounted onto microscope slides. For nuclear counterstaining, cells were incubated with TOPRO-3 (Molecular Probes). For γ-H2AX and BrdU co-staining, cells were fixed and permeabilized. To denature DNA, fixed cells were resuspended in 4 N HCl and incubated for 30 min at 37 °C. After washing with borate buffer and phosphate-buffered saline (PBS) to remove any acid traces, cells were simultaneously incubated with a mouse anti-BrdU antibody and a rabbit anti-γ-H2AX antibody. Primary antibodies were detected with a secondary Alexa 546-conjugated goat, anti-mouse antibody and a secondary Alexa 488-conjugated goat, anti-rabbit antibody. Images were obtained with either a Leica TCS SP5 laser-scanning confocal microscope (Leica, Wetzlar, Germany) or with a FluoView Olympus laser-scanning confocal microscope (Olympus, Tokyo, Japan). Images were transferred to Adobe Photoshop CS4 (Adobe Systems) for assembly.

Transmission electron microscopy. Immunolabeling was performed on formaldehyde-fixed and Lowicryl-K4M-embedded cells as described previously.[37] For ultrastructure, samples were washed in Sörensen's buffer and fixed for 1 h at 4 °C with 2.5% glutaraldehyde in Sörensen's 0.1 M phosphate buffer (pH 7.4), and post-fixed for 30 min with 1% osmium tetroxide. After dehydration in graded ethanol, samples were embedded in Epon. Ultrathin sections obtained with a Reichert Ultracut S ultramicrotome were contrasted with uranyl acetate and lead citrate. Observations were made with a Jeol 100 CX II transmission electron microscope at 60 kV.

MNaseI sensitivity assay. MCF-7 cells (1×10^6) were Dounce-homogenized in RSB buffer (10 mmol/l Tris-HCl (pH 7.4), 10 mM NaCl, 3 mM $MgCl_2$, 0.5% NP-40) containing 10 μg/ml aprotinin and leupeptin, 1 mM phenylmethylsulfonyl fluoride, 1 mM Na_3VO_4, and 1 mM dithiothreitol (DTT), and incubated on ice for 15 min. Samples were centrifuged at 4 °C for 5 min at 1400 $\times$ *g*, the medium was removed, samples were washed twice with RSB buffer, and digested with 0.25 to 2.5 U of micrococcal nuclease in digestion buffer (15 mM Tris-HCl (pH 7.5), 60 mM KCl, 15 mM NaCl, 1 mM $CaCl_2$, 3 mM $MgCl_2$, 20% glycerol, 15 mM β-mercaptoethanol) for 5 min. Digestion was stopped by adding 1 volume of stop solution (50 mM Tris (pH 7.5), 150 mM NaCl, 50 mM EDTA, 0.3% sodium dodecyl sulfate (SDS)). DNA was extracted using 1 volume of phenol/chloroform/isoamyl alcohol (25 : 24 : 1) followed by 1 volume chloroform/isoamyl alcohol (24 : 1) and precipitated with 100% ethanol. DNA was washed once with 70% ethanol, resuspended in H_2O, and 1.5 μg of DNA was separated using 1.2% agarose gel.

Chromatin isolation. Chromatin fractionation was performed as described previously.[38] Three different fractions were collected: cytoplasmic fraction (S2), nuclear soluble proteins (S3), and chromatin-enriched fraction (P3).

Western blot analysis. Adherent (and floating depending on the experiment) cells were lysed into an SDS buffer (SDS 1%, Tris-HCl 40 mM (pH 7.5), EDTA 1 mM, protease inhibitor mixture) unless otherwise stated. Equal amounts of proteins were resolved by SDS-PAGE. Membranes were probed with primary antibodies, followed by horseradish peroxidase (HRP)-conjugated secondary antibodies, and developed by chemiluminescence detection.

WST-1 cell viability. Cell survival was determined by WST-1 (2-(4-iodophenyl)-3-(4-nitrophenyl)-5-(2,4-disulfophenyl)-2H-tetrazolium, monosodium salt) cell viability assay according to the manufacturer's instructions (Roche, Basel, Switzerland).

Cell-cycle analysis. The relative percentage of cells in each stage of the cell cycle was analyzed according to the procedure of labeling nuclei with propidium iodide (PI) followed by flow cytometric analysis using FACSCalibur II and the ModFit LT program.

***In vitro* DNA content measurement.** Fluorimetric DNA titration was performed as described previously.[39]

***In vivo* DNA replication assay.** Cells were labeled with 33 μM BrdU for 30 min, resuspended in PBS + 10% FBS, and then fixed with 70% cold ethanol. DNA was denatured with 4 N HCl + 0.5% Triton X-100 for 30 min at 37 °C. After washing cells with PBS, the pellet was resuspended in PBS + 10% FBS. An anti-BrdU antibody (clone BU-33; Sigma) was added and cells were incubated for 1 h at room temperature. After washing, an Alexa 488-conjugated goat, anti-mouse secondary antibody (Molecular Probes) was added for 1 h at room temperature in dark. After washing, cells were collected, resuspended in PI solution (EDTA 3 mM (pH 8.0), Tween 20 0.05%, PI 50 μg/ml, RNAse A 50 μg/ml in PBS), and analyzed using a FACSCalibur II and the CellQuest software (BD Biosciences).

DNA fiber assay. Cells were doubly labeled by incubating with 50 μM iododeoxyuridine (IdU) for 20 min followed by incubation with 50 μM chlorodeoxyuridine (CldU) for 30 min. A 2-μl volume of cells, resuspended in ice-cold PBS at 10^6 cells/ml, was spotted onto a silane-coated microscope slide (Sigma) and then overlaid with 10 μl of spreading buffer (SDS 0.5%, Tris-HCl 200 mM (pH 7.4), EDTA 50 mM). After 6 min, the slides were tilted by 15 degrees to allow lysates to slowly move down the slide. The DNA spreads were air-dried, fixed in a 3 : 1 mixture of methanol/acetic acid for 15 min at −20 °C, and stored in pre-chilled 70% ethanol at 4 °C overnight. The slides were then treated with 4 M HCl for 10 min at room temperature followed by 30 min at 37 °C in a water bath, washed three times in PBS, and incubated in blocking buffer (2% BSA in PBS) for 1 h at room temperature followed by 1 h at 37 °C with a rat anti-BrdU antibody (to detect CldU) (clone BU1/75; AbDSerotec) plus a mouse anti-BrdU (to detect IdU) (clone B44; BD Biosciences). After rinsing three times with stringency buffer (Tris-HCl 10 mM (pH 7.5), NaCl 400 mM, Tween 20 0.1%, NP-40 0.1%) the slides were incubated for 1 h with Alexa Fluor 488-conjugated rabbit, anti-mouse antibodies and Alexa Fluor 546-conjugated goat, anti-rat antibodies (Molecular Probes). Slides were rinsed three times with PBS, once with H_2O, and mounted in Mowiol medium. Microscopy was performed using a FluoView Olympus laser-scanning confocal microscope using the sequential scanning mode. A single-blind evaluation was performed to measure the lengths of continuously double-stained tracks using the ImageJ software (NCI/NIH, Bethesda, MD, USA) and the collected images were processed using the Adobe Photoshop CS4 software (Adobe Systems). Pictures were taken on the entire slide and on multiple slides, reducing the chance of over- or under-representing certain origins or genomes of individual cells. Micrometer values were converted into kilobase using the conversion factor 1 μm = 2.59 kb. Measurements were recorded from fibers in well-spread (untangled) areas of the slides to prevent the possibility of recording labeled patches from bundles of fibers.

Isolation of nascent-strand DNA. Isolation of nascent-strand DNA was performed as described previously.[40] The primers and PCR conditions are described by Rampakakis *et al.*[40]

Annexin V staining. Apoptotic cells were determined by Annexin V–FITC (fluorescein isothiocyanate) and non-vital dye PI staining using an FITC–Annexin V apoptosis detection kit I (BD Biosciences) according to the manufacturer's instructions. Flow cytometry was performed using a FACSCanto and samples were analyzed using the CellQuest software (BD Biosciences). Both Annexin V^+/PI^- cells representing early-apoptotic cells and Annexin V^+/PI^+ mostly representing late-apoptotic/necrotic cells were considered as apoptotic cells.

CAM tumor model. A window was opened in the eggshell of a 3-day-old embryo using scissors after puncturing the air chamber. The window was sealed with tape and the eggs were incubated at 37 °C and 80% humidity until cell grafting. Eight days later, a Matrigel/cell mixture (1 : 1) was grafted within a plastic ring on the CAM surface. The window was sealed and eggs were incubated under the same conditions for 7 days. On day 18, tumors were dissected and diameters were measured with a caliper. Tumor volume was calculated using an ellipsoid formula: Volume $(mm^3) = (4 \times \pi \times Z_1 \times Z_2 \times Z_3)/3$, where Z_{1-3} are the main radii of the tumor.

Statistical analyses. Results were reported as means with their S.D. or S.E.M. as reported in the figure legends. Statistical analysis was performed by one-way ANOVA or two-way ANOVA regarding the number of grouping factors. Group means were compared by Bonferroni's post-test. Homoscedasticity was assayed by Levene's test. Normality was assayed by the D'Agostino and Pearson test. All tests were performed with a 95% interval of confidence.

Conflict of Interest

The authors declare no conflict of interest.

Acknowledgements. This work was supported by grants from the National Fund for Scientific Research (FNRS) (Belgium), the Centre Anti-Cancéreux près de l'Université de Liège, the Fonds Léon Frédéricq, and TELEVIE. D Mottet and F Dequiedt are Research Associates at the National Fund for Scientific Research (FNRS). M Boxus is Postdoctoral Researcher at the FNRS. N Matheus is an FRIA Fellow. A Gonzalez is TELEVIE Fellow. We thank Dr D DiPaola for expert advice on the nascent-strand DNA abundance assay.

1. de Ruijter AJ, van Gennip AH, Caron HN, Kemp S, van Kuilenburg AB. Histone deacetylases (HDACs): characterization of the classical HDAC family. *Biochem J* 2003; **370** (Part 3): 737–749.
2. Bertrand P. Inside HDAC with HDAC inhibitors. *Eur J Med Chem* (2010); **45**: 2095–2116.
3. Duvic M, Vu J. Vorinostat: a new oral histone deacetylase inhibitor approved for cutaneous T-cell lymphoma. *Expert Opin Investig Drugs* 2007; **16**: 1111–1120.
4. Mottet D, Pirotte S, Lamour V, Hagedorn M, Javerzat S, Bikfalvi A *et al.* HDAC4 represses p21(WAF1/Cip1) expression in human cancer cells through a Sp1-dependent, p53-independent mechanism. *Oncogene* 2009; **28**: 243–256.
5. Wilson AJ, Byun DS, Nasser S, Murray L, Ayyanar K, Arango D *et al.* HDAC4 promotes growth of colon cancer cells via repression of p21. *Mol Biol Cell* 2008; **19**: 4062–4075.
6. Zhu C, Chen Q, Xie Z, Ai J, Tong L, Ding J *et al.* The role of histone deacetylase 7 (HDAC7) in cancer cell proliferation: regulation on c-Myc. *J Mol Med* 2011; **89**: 279–289.
7. Kitamura Y, Shimizu K, Tanaka S, Ito K, Emi M. Allelotyping of anaplastic thyroid carcinoma: frequent allelic losses on 1q, 9p, 11, 17, 19p, and 22q. *Genes Chromosomes Cancer* 2000; **27**: 244–251.
8. Scanlan MJ, Welt S, Gordon CM, Chen YT, Gure AO, Stockert E *et al.* Cancer-related serological recognition of human colon cancer: identification of potential diagnostic and immunotherapeutic targets. *Cancer Res* 2002; **62**: 4041–4047.
9. Ozdag H, Teschendorff AE, Ahmed AA, Hyland SJ, Blenkiron C, Bobrow L *et al.* Differential expression of selected histone modifier genes in human solid cancers. *BMC Genomics* 2006; **7**: 90.
10. Bradbury CA, Khanim FL, Hayden R, Bunce CM, White DA, Drayson MT *et al.* Histone deacetylases in acute myeloid leukaemia show a distinctive pattern of expression that changes selectively in response to deacetylase inhibitors. *Leukemia* 2005; **19**: 1751–1759.
11. Osada H, Tatematsu Y, Saito H, Yatabe Y, Mitsudomi T, Takahashi T. Reduced expression of class II histone deacetylase genes is associated with poor prognosis in lung cancer patients. *Int J Cancer* 2004; **112**: 26–32.
12. Milde T, Oehme I, Korshunov A, Kopp-Schneider A, Remke M, Northcott P *et al.* HDAC5 and HDAC9 in medulloblastoma: novel markers for risk stratification and role in tumor cell growth. *Clin Cancer Res* 2010; **16**: 3240–3252.
13. Van Hooser A, Goodrich DW, Allis CD, Brinkley BR, Mancini MA. Histone H3 phosphorylation is required for the initiation, but not maintenance, of mammalian chromosome condensation. *J Cell Sci* 1998; **111** (Part 23): 3497–3506.
14. Singer JD, Gurian-West M, Clurman B, Roberts JM. Cullin-3 targets cyclin E for ubiquitination and controls S phase in mammalian cells. *Genes Dev* 1999; **13**: 2375–2387.
15. Ahn JY, Schwarz JK, Piwnica-Worms H, Canman CE. Threonine 68 phosphorylation by ataxia telangiectasia mutated is required for efficient activation of Chk2 in response to ionizing radiation. *Cancer Res* 2000; **60**: 5934–5936.
16. Feijoo C, Hall-Jackson C, Wu R, Jenkins D, Leitch J, Gilbert DM *et al.* Activation of mammalian Chk1 during DNA replication arrest: a role for Chk1 in the intra-S phase checkpoint monitoring replication origin firing. *J Cell Biol* 2001; **154**: 913–923.
17. Falk M, Lukasova E, Kozubek S. Higher-order chromatin structure in DSB induction, repair and misrepair. *Mutat Res* 2010; **704**: 88–100.
18. Kim MS, Blake M, Baek JH, Kohlhagen G, Pommier Y, Carrier F. Inhibition of histone deacetylase increases cytotoxicity to anticancer drugs targeting DNA. *Cancer Res* 2003; **63**: 7291–7300.
19. Ahringer J. NuRD and SIN3 histone deacetylase complexes in development. *Trends Genet* 2000; **16**: 351–356.
20. Sims JK, Wade PA. Mi-2/NuRD complex function is required for normal S phase progression and assembly of pericentric heterochromatin. *Mol Biol Cell* 2011; **22**: 3094–3102.

21. David G, Turner GM, Yao Y, Protopopov A, DePinho RA. mSin3-associated protein, mSds3, is essential for pericentric heterochromatin formation and chromosome segregation in mammalian cells. *Genes Dev* 2003; **17**: 2396–2405.
22. Rountree MR, Bachman KE, Baylin SB. DNMT1 binds HDAC2 and a new co-repressor, DMAP1, to form a complex at replication foci. *Nat Genet* 2000; **25**: 269–277.
23. Bhaskara S, Chyla BJ, Amann JM, Knutson SK, Cortez D, Sun ZW *et al.* Deletion of histone deacetylase 3 reveals critical roles in S phase progression and DNA damage control. *Mol Cell* 2008; **30**: 61–72.
24. Conti C, Leo E, Eichler GS, Sordet O, Martin MM, Fan A *et al.* Inhibition of histone deacetylase in cancer cells slows down replication forks, activates dormant origins, and induces DNA damage. *Cancer Res* 2010; **70**: 4470–4480.
25. Bierne H, Tham TN, Batsche E, Dumay A, Leguillou M, Kerneis-Golsteyn S *et al.* Human BAHD1 promotes heterochromatic gene silencing. *Proc Natl Acad Sci USA* 2009; **106**: 13826–13831.
26. Heo K, Kim B, Kim K, Choi J, Kim H, Zhan Y *et al.* Isolation and characterization of proteins associated with histone H3 tails *in vivo*. *J Biol Chem* 2007; **282**: 15476–15483.
27. Lemercier C, Brocard MP, Puvion-Dutilleul F, Kao HY, Albagli O, Khochbin S. Class II histone deacetylases are directly recruited by BCL6 transcriptional repressor. *J Biol Chem* 2002; **277**: 22045–22052.
28. Zhang CL, McKinsey TA, Olson EN. Association of class II histone deacetylases with heterochromatin protein 1: potential role for histone methylation in control of muscle differentiation. *Mol Cell Biol* 2002; **22**: 7302–7312.
29. Seiler JA, Conti C, Syed A, Aladjem MI, Pommier Y. The intra-S-phase checkpoint affects both DNA replication initiation and elongation: single-cell and -DNA fiber analyses. *Mol Cell Biol* 2007; **27**: 5806–5818.
30. Willis N, Rhind N. Regulation of DNA replication by the S-phase DNA damage checkpoint. *Cell Div* 2009; **4**: 13.
31. Lee H, Larner JM, Hamlin JL. A p53-independent damage-sensing mechanism that functions as a checkpoint at the G_1/S transition in Chinese hamster ovary cells. *Proc Natl Acad Sci USA* 1997; **94**: 526–531.
32. Mathew R, Kongara S, Beaudoin B, Karp CM, Bray K, Degenhardt K *et al.* Autophagy suppresses tumor progression by limiting chromosomal instability. *Genes Dev* 2007; **21**: 1367–1381.
33. McPherson JP, Lemmers B, Chahwan R, Pamidi A, Migon E, Matysiak-Zablocki E *et al.* Involvement of mammalian Mus81 in genome integrity and tumor suppression. *Science* 2004; **304**: 1822–1826.
34. Marchion DC, Bicaku E, Turner JG, Schmitt ML, Morelli DR, Munster PN. HDAC2 regulates chromatin plasticity and enhances DNA vulnerability. *Mol Cancer Ther* 2009; **8**: 794–801.
35. Marchion DC, Bicaku E, Daud AI, Sullivan DM, Munster PN. Valproic acid alters chromatin structure by regulation of chromatin modulation proteins. *Cancer Res* 2005; **65**: 3815–3822.
36. Waltregny D, Glenisson W, Tran SL, North BJ, Verdin E, Colige A *et al.* Histone deacetylase HDAC8 associates with smooth muscle alpha-actin and is essential for smooth muscle cell contractility. *FASEB J* 2005; **19**: 966–968.
37. Vandelaer M, Thiry M. The phosphoprotein pp135 is an essential constituent of the fibrillar components of nucleoli and of coiled bodies. *Histochem Cell Biol* 1998; **110**: 169–177.
38. Mendez J, Stillman B. Chromatin association of human origin recognition complex, cdc6, and minichromosome maintenance proteins during the cell cycle: assembly of prereplication complexes in late mitosis. *Mol Cell Biol* 2000; **20**: 8602–8612.
39. Labarca C, Paigen K. A simple, rapid, and sensitive DNA assay procedure. *Anal Biochem* 1980; **102**: 344–352.
40. Rampakakis E, Di Paola D, Zannis-Hadjopoulos M. Ku is involved in cell growth, DNA replication and G_1–S transition. *J Cell Sci* 2008; **121** (Part 5): 590–600.

Supplementary Information accompanies the paper on Cell Death and Differentiation website (http://www.nature.com/cdd)